Synthetic analysis of periodically stimulated excitable and oscillatory membrane models

K. Yoshino,* T. Nomura, K. Pakdaman, and S. Sato
Department of Systems and Human Science, Graduate School of Engineering Science, Osaka University, Toyonaka 560-8531, Osaka, Japan
(Received 10 April 1998)

Many excitable neuronal membranes become oscillatory when stimulated by large enough dc currents. In this paper we investigate how the transition from excitable to oscillatory regimes affects the response of the membrane to periodic pulse trains. To this end, we examine how the dynamics of periodically stimulated FitzHugh-Nagumo neuron model changes as the system switches from excitability to oscillation. We show that, despite the important change in the asymptotic dynamics of the unperturbed model, $p:q$ phase-locking (i.e., the model membrane discharges q times in p interstimulus intervals and q input-output intervals repeat periodically) regions in the stimulus period-stimulus amplitude parameter plane (Arnold tongues) change continuously when the model changes from excitable to oscillatory. We provide further evidence for the continuous change of the Arnold tongues by using an analytically tractable one-dimensional map that approximates the Poincaré map of the forced system. We argue that the smooth change in the Arnold tongues results from the fact that, despite the qualitative difference between the asymptotic dynamics of unforced excitable and oscillatory regimes, other aspects of the dynamics such as the wave form of individual action potentials, are similar in the two regimes. [S1063-651X(99)04701-7]

PACS number(s): 87.10.+e, 87.19.La

I. INTRODUCTION

Neuron membranes generate brief electrical pulses, referred to as ''spikes,'' the dominant carrier of information in nervous systems [1]. Many neuron membranes are excitable. Their membrane potential stabilizes at a constant value in the absence of perturbation. Following a pulselike perturbation, the membrane potential returns to its steady state either directly when the pulse amplitude is below some threshold or after a large excursion, i.e., the action potential, when the pulse is above threshold [2,3]. Many excitable membranes become oscillatory in response to large enough dc current stimulation, that is, they generate a regular train of action potentials.

Models such as the Hodgkin-Huxley (HH) equations [4] and FitzHugh-Nagumo (FHN) equations [5] reproduce successfully the two types of membrane behavior. In these models, the sudden change from excitability to oscillation and vice versa is obtained by modifying the value of parameters representing temperature, conductance of ions, concentration of each ion, intensity of current stimulation, and so on, across critical values [6]. From the point of view of dynamical system theory, this abrupt transition is a bifurcation [7,8].

Figure 1 exemplifies membrane potential wave forms of the HH equations in response to a step current stimulation with different intensities. The intensity of the current reaches a bifurcation point between Figs. 1(c) and 1(d), where the membrane model transits from excitable to oscillatory. The bifurcation is called a double cycle and for the parameter value above the bifurcation point a stable limit cycle exists.

In this paper we investigate how the dynamics of a neuronal model stimulated by periodic impulsive inputs changes when the system switches from excitability to oscillations. Previous experimental and theoretical studies of periodically stimulated neurons as well as cardiac muscle cells have mainly concentrated on the description of the dynamics of forced systems in either the excitable or the oscillatory regimes [9–15] and the effect of parameters changes *within* each of them [9]. To our knowledge, no attempt has been made to see how the two relate to each other, that is, how the response is changed when one parameter is moved across the bifurcation point separating excitability from oscillation.

In our previous works we showed that both the oscillatory and excitable membrane models exhibit slow and fast changes of the membrane potential, respectively, in the sub- and suprathreshold regions and this property is responsible for the fact that neuronal models such as the FHN equations can mimic living neurons' responses to external stimulation [15]. Here, using this model we show that $p:q$ phase locking (i.e., the model membrane discharges q times in p interstimulus intervals and q input-output intervals repeat periodically) regions in the two-parameter plane (Arnold tongues) change continuously ''when the intrinsic dynamics of the model (i.e., dynamics of the model without external forcing) [changes] from excitable to oscillatory.'' We abbreviate this quoted phrase as *along the transition* in the following.

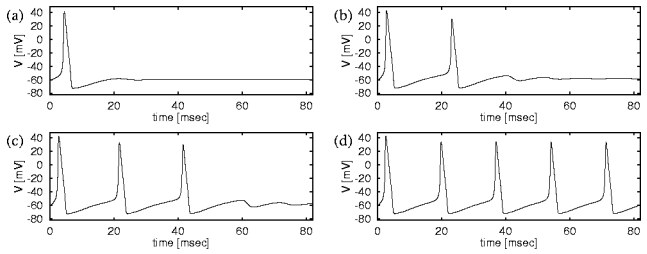

FIG. 1. Wave forms of the HH equations and membrane potential V (mV) versus time (ms) in response to step current I applied at time 0 with different intensities. $I=0$ (μA/cm^2) for $t<0$. (a) $I=3.2$ (μA/cm^2), single spike; (b) $I=6.0$ (μA/cm^2), double spike; (c) $I=6.2$ (μA/cm^2), triple spike; and (d) $I=7.0$(μA/cm^2), periodic firing.

*Electronic address: yoshino@bpe.es.osaka-u.ac.jp

The dynamics of periodically forced nonlinear systems can be described by that of the corresponding Poincaré maps. When the unforced model possesses a limit cycle, it is possible to approximate the Poincaré maps by one-dimensional maps [11,16]. Various kinds of one-dimensional maps including circle maps have been studied in the field of biological rhythms and neuronal modeling [11,17]. We define appropriate one-dimensional maps to describe the dynamics of both the oscillatory and excitable membrane models stimulated by periodic pulse trains. This is possible by extending the concepts of phase and isochron utilized for oscillatory systems to excitable systems [18]. Then the changes in the two-parameter bifurcation diagrams can be understood by changes in the shape of the one-dimensional maps.

Section II introduces the FHN model as an excitable-oscillatory membrane model. In Sec. III we show the dynamics of the FHN equations driven by periodic pulse trains and observe that their global organization of the dynamics in the parameter space changes continuously along the transition. Then, in Sec. IV we analyze the dynamics displayed in Sec. III by using one-dimensional maps that approximate Poincaré maps of the periodically forced system. In Sec. V we further show that the continuous change of the Arnold tongues can be clearly understood by using an analytically tractable one-dimensional map. Finally, we discuss our results in Sec. VI.

II. EXCITABLE-OSCILLATORY MEMBRANE MODEL

FitzHugh-Nagumo equations are a theoretical model for an excitable-oscillatory membrane [5]:

$$\dot{x} = c(x - x^3/3 - y + z),$$

$$\dot{y} = \frac{1}{c}(x - by + a). \tag{2.1}$$

The variable x represents the membrane potential of the neuron, y the refractoriness. The parameter z represents the current stimulation to the membrane model. It corresponds to the externally applied current intensity changed as the parameter in Fig. 1 in the HH equations. z is treated as the constant dc current and changed as an intrinsic parameter in this paper. We set $a = 0.7$, $b = 0.8$, and $c = 3.0$ throughout the paper.

Let us illustrate the phase portrait of the model and how it changes depending on the parameter value z. When z is close to zero, the system has a unique equilibrium point (resting point P) that is either a stable node or a stable focus. The model behaves as an excitable membrane. Figure 2(a) shows the corresponding phase portrait with trajectories from several initial states. A strong enough excitatory stimulation delivered to the system at the resting (equilibrium) point P displaces it rightward beyond the quasitype (QTP) separatrix (i.e., threshold) and leads to an action potential. If the stimulus is below threshold, the state point returns to P without passing through the active region. All trajectories in the plane first approach the thick curve referred to as the *reference trajectory* (RT) and then asymptotically approach the equilibrium P along the RT [19].

As the z value increases, the focal equilibrium becomes less attractive and trajectories near the equilibrium consist of

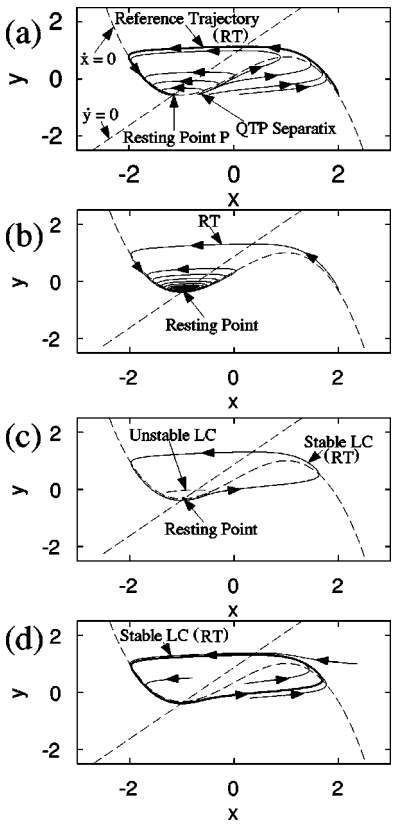

FIG. 2. x-y phase portraits of the FHN equations with several values of the parameter z: (a) $z = 0.1$, an excitable membrane with a small spiral; (b) $z = 0.3368$, an excitable membrane with a big spiral; (c) $z = 0.338$, bistable with a stable equilibrium point and a stable limit cycle; and (d) $z = 0.347$, an oscillatory membrane. In (c) and (d), LC denotes a limit cycle. The units of x, y and z are arbitrary.

big spirals [Fig. 2(b)]. In this case, each trajectory first moves toward the equilibrium along the RT as in Fig. 2(a). However, since the equilibrium is less stable than in Fig. 2(a), it winds with a relatively large radius around the equilibrium and finally converges to the equilibrium. As z increases further, a neutral stable limit cycle (inside unstable and outside stable) appears abruptly through a double cycle bifurcation. Then stable and unstable limit cycles are generated [Fig. 2(c)], leading to bistability. The double cycle bifurcation constitutes the boundary separating the excitable and oscillatory regimes. Finally, for still larger z, the stable equilibrium point loses its stability (the Hopf bifurcation) and the system shows the monostable limit cycle oscillation [Fig. 2(d)]. Figure 3 summarizes these changes of the dynamics as a function of the parameter z.

III. ARNOLD TONGUES OF THE PERIODICALLY STIMULATED FHN EQUATIONS

In this section we simulate the dynamics of the FHN stimulated by periodic pulse trains and characterize them in the two-parameter plane, i.e., the intensity A and the stimulus period T.

A. Phase locking and chaotic responses

Phase lockings are typical dynamics of periodically forced nonlinear systems. This is also the case for the neu-

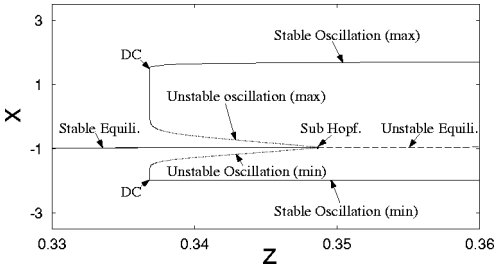

FIG. 3. One-parameter bifurcation diagram of the FHN equations. The steady states of the system are described. The abscissa is the parameter z representing the constant dc current. The ordinate is the variable x, the membrane potential. The center curve represents the equilibrium potential, and the upper and lower curves represent the maximum and minimum values of oscillating membrane potentials, respectively. Solid and dashed lines represent stable and unstable oscillations, respectively. The dotted line is for unstable equilibrium potential. Sub Hopf. and DC are the subcritical Hopf and the double cycle bifurcation points, respectively. The units of x and z are arbitrary.

ronal membrane model. If the membrane model fires periodically q times every p successive pulses and each stimulus-firing interval is locked, the response is referred to as $p:q$ phase locking. The period of the dynamics is pT, where T is a period of the input train.

Figure 4 exemplifies the responses of the FHN equations to periodic pulse trains. We assume the duty cycle of the periodic pulse (i.e., the length of the pulse in each cycle) to be zero throughout the paper. That is, each pulse shifts instantaneously the membrane potential x to $x+A$. In each of the phase portraits in Figs. 4(a)–4(d), the trajectory forms a closed curve, which indicates that the dynamics are periodic. For example, Fig. 4(a) displays the 3:1 phase locking response. It is hard to recognize from the figure whether the intrinsic dynamics of the model is excitable or oscillatory. This implies that the forced dynamics of both the excitable and oscillatory models possess response characteristics common to the periodic stimulation. Indeed, the model is excitable in Figs. 4(a)–4(c) and oscillatory in Fig. 4(d). Since the model's equilibrium is a less attractive focus in Figs. 4(b) and 4(c), the trajectory winds several times around the equilibrium between successive spikes and the corresponding waveforms resemble a seesaw in the subthreshold region. In Figs. 4(e) and 4(f) the trajectory does not form a closed curve and the responses are chaotic.

B. Arnold tongues

The dynamics of periodically forced nonlinear systems depends on parameter values of forcing inputs as well as the system's intrinsic parameter values. In our case, the former parameters are the period T and the intensity A of the input trains and the latter is the parameter z.

In Fig. 5 we summarize the dependence of the model's dynamics on these parameters. For arbitrary but fixed values of z, the two-parameter plane (T,A) is divided into several regions. In each region, the qualitative dynamics of the model are identical. The diagram is called the two-parameter bifurcation diagram (2BD). The parameter value z increases from top [Fig. 5(a) to bottom Fig. 5(e)]. That is, the intrinsic dynamics of the model undergoes the transition from excitable to oscillatory. $p:q$ phase locking regions are indicated by their locking ratio.

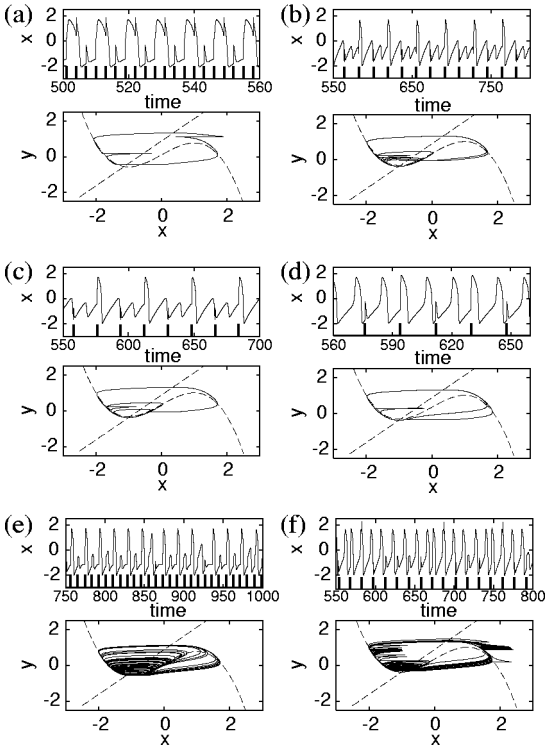

FIG. 4. Wave forms of the model in response to periodic pulse trains (upper traces) and the corresponding trajectories in the x-y phase plane (lower panels) for different values of z, A, and T. Since the model's variables and parameters are dimensionless, the units of the variables and time axes are arbitrary. The parameter values of z in (a) and (e) correspond to that in Fig. 2(a). The values of z in (b) and (c) correspond to that in Fig. 2(b). The values of z in (d) and (f) correspond to that in Fig. 2(d). The parameter values A and T are as follows: (a) $A=1.5$ and $T=3.0$, 3:1 phase locking response; (b) $A=1.0$ and $T=18.2$, 4:2 phase locking response; (c) $A=0.9$ and $T=18.0$, 2:1 phase locking response; (d) $A=1.5$ and $T=18.0$, 2:3 phase locking response; (e) $A=0.6732$ and $T=9.0$, chaotic response; (f) $A=1.0$ and $T=14.9492$, chaotic response.

Figure 5 includes several well-known bifurcation structures explored experimentally in electrophysiology [13] and in numerical simulations of neuronal or muscle cell models [11,12,14,15] and electrical circuits [20]. In the rest of this section we roughly illustrate several main features of 2BDs and their z-value dependence. For some statements, we ignore small regions and the detailed structure of the diagrams. In Fig. 5(a) the intrinsic dynamics of the model are excitable. The organization of Fig. 5(a) is quite similar to that obtained in the periodically stimulated squid giant axon [13]. For low intensities A, the model does not exhibit firing (0 response region) [21]. For higher intensities, the dominant region is 1:1. Then the 2:1 and 3:1 regions follow it. Between $p:q$ and $p':q',(p+p'):(q+q')$ is subdominant and there exist more complicated phase locking and nonlocking response regions including period doubling cascades to chaos [14].

Figure 5(e) is for the oscillatory membrane model with the monostable limit cycle. In this case, there is no 0 response region since the model membrane fires spontaneously without inputs. The phase locking regions are known as Arnold tongues. The value of the input period at the lowest

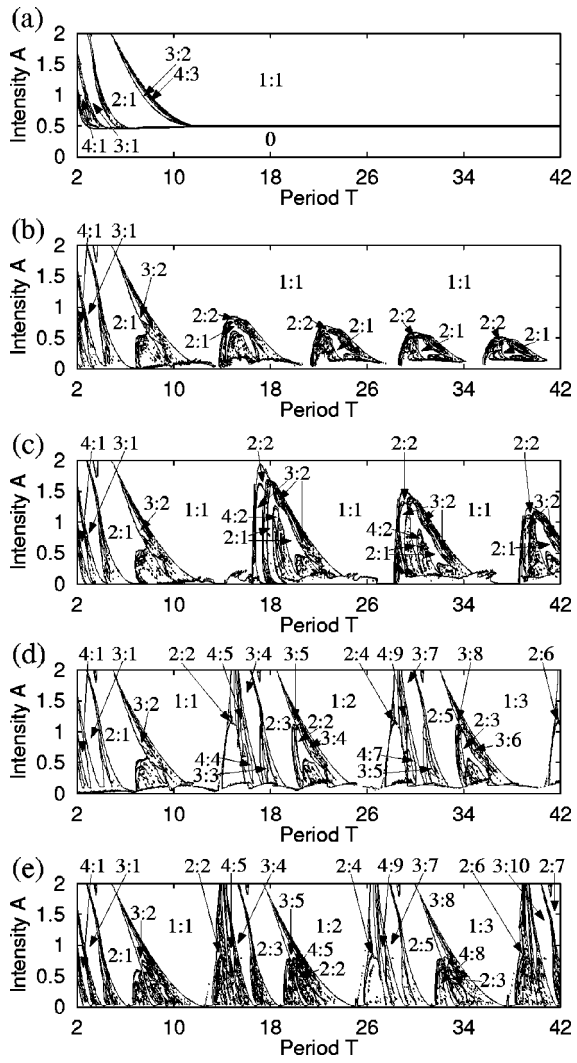

FIG. 5. Two-parameter bifurcation diagrams of the FHN equations stimulated by periodic pulse trains for several values of constant dc current z. The ordinate is the pulse intensity A and the abscissa is the period T. The diagrams are obtained numerically using the fourth-order Runge-Kutta method ($\triangle t=0.01$). The dominant p:q phase locking regions ($p=1,2,3,4$ and $q=1,2,\ldots$) are labeled by their locking ratio; nonlabeled regions include narrow locking regions with period 4 or higher and nonlocking (i.e., chaotic or quasiperiodic) responses. The parameter value z are (a) $z=0.1$ (excitable with a small spiral), (b) $z=0.335$ (excitable with a big spiral), (c) $z=0.3368$ (excitable with a big spiral), (d) $z=0.338$ (bistable), and (e) $z=0.347$ (oscillatory with the monostable limit cycle). The units of z and the axes are arbitrary.

apex of the 1:1 region coincides with the natural period of the unperturbed intrinsic oscillation, say N, and that of 1:2 is twice as large, i.e., $2N$. The global organization of the diagram shows a repeated structure with period N in the horizontal direction. As in Fig. 5(a), between p:q and p':q', $(p+p')$:$(q+q')$ is subdominant and chaotic response regions are also observed.

Our finding in Fig. 5 is that the diagram changes continuously as the model's intrinsic parameter z varies. In Fig. 5(a) all the bifurcation curves seem to asymptotically approach the boundary that separates the 0 response region from the other regions. This implies that various kind of dynamics degenerate along the boundary. As the z value increases [Fig. 5(b)], this boundary moves downward gradually, reflecting the fact that the threshold of the model becomes lower. Moreover, the phase lockings with higher periods and chaotic response regions that constitute ''mountains'' and ''valleys'' begin to appear along the boundary, indicating that the degeneracy in Fig. 5(a) is unfolded. The dominant phase locking regions such as 1:1 and 2:1 for higher intensities remain similar to those in Fig. 5(a). Figures 5(b) and 5(c) show that for a fixed z, the mountains become lower and the intervalley intervals become shorter as the stimulus period T increases. As z increases from Fig. 5(b) to 5(c), the mountains become higher and the intervalley intervals become larger. Further increasing the value of z above the double cycle bifurcation point, intervalley intervals coincide with the natural period of the oscillation N and the bifurcation structure gains periodicity as observed in the Figs. 5(d) and 5(e) for the periodically forced oscillatory membrane model. Note the nonlabeled region along the bottom of Fig. 5(d). The lower portion of this region is the 0 response region in which the state point remains inside the unstable limit cycle (basin of attraction of the equilibrium point). Some of the subthreshold dynamics are periodic and some are chaotic [21]. In the upper part of this region, the model shows periodic or aperiodic burstinglike firings (figures not shown). When the model is in the active phase of the bursts, the state point moves along the stable limit cycle. The state point is kicked inside the unstable limit cycle by a stimulus, leading to the silent phase of the bursts. These dynamics are due to the bistability of the intrinsic dynamics of the model [22].

IV. ONE-DIMENSIONAL MAP ANALYSIS

The dynamics of periodically forced nonlinear systems is usually analyzed by Poincaré maps that describe sequential dynamics of the system's state at a fixed phase of the periodic forcing [7]. In this section we analyze the dynamics illustrated in Sec. III by using one-dimensional maps that approximate Poincaré maps of the system.

A. Definition of one-dimensional maps

In this subsection we first define the phase for the oscillatory FHN equations to describe the system's state. Then we extend the phase for the oscillatory system to that for the excitable one. This enables us to construct one-dimensional maps that approximate the Poincaré maps of the periodically stimulated FHN equations.

Let $X=(x,y)$ denote a state point in the two-dimensional phase plane of the model. If a limit cycle γ of the FHN equations is stable, then

$$\forall\ \overline{X}\in\gamma,\ \exists\ \{t_i\}\quad (i=1,2,\ldots),$$

$$\Phi(X,t_i)\rightarrow\overline{X}\in\gamma\quad \text{as}\ \ i\rightarrow\infty, \tag{4.1}$$

where $t_1<t_2<\cdots<t_i<\cdots$ and $t_i\rightarrow\infty$ as $i\rightarrow\infty$. $\Phi(X,t)$ represents the system's flow and X is in the basin of attraction of γ. $\overline{X}$ is the ω-limit point of X [7]. When X is appropriately chosen and $t_i=iN$, where N is the natural period of the os-

cillation, the set of convergent sequences leads to the concept of the isochron $W^s(\overline{X})$ ($\overline{X}\in\gamma$), a stable manifold [3,23].

$$W^s(\overline{X})=\{X';\lim_{t\to\infty}\|\Phi(X',t)-\Phi(\overline{X},t)\|\to 0,\overline{X}\in\gamma\}. \tag{4.2}$$

This means that $\Phi(X',t)$ starting from X' in the isochron $W^s(\overline{X})$ and $\Phi(\overline{X},t)$ starting from $\overline{X}\in\gamma$ asymptotically approach each other and eventually, after a long enough time, become indistinguishable.

We define the phase on the limit cycle γ so that the state $X\in\gamma$ can be described by its phase $\phi(X)$, where $\phi:\gamma\to S^1$. The phase of $X\in\gamma$ for the FHN equations is defined as follows: $\phi(X)=0$ when X is at the point where the membrane potential attains its maximum value (peak of the action potential) along γ. We call this point the datum point. Let t be the time necessary to reach X starting from the datum point and moving along γ; then $\phi(X)$ is defined as $t \pmod N$.

These two concepts, namely, the isochron and the phase, lead naturally to the definition of one-dimensional maps that describe responses of the limit cycle oscillator to an impulsive perturbation. Suppose that a stimulus with intensity A is applied to the system at $X\in\gamma$ whose phase is $\phi(X)$. Then X is displaced by an amount A to the point $X'\in W^s(X'')$ for some $X''\in\gamma$. Since X' is eventually identified with $X''\in\gamma$, the phase of the system will be shifted eventually to $\phi(X'')$. The amount of phase shift $\phi(X)-\phi(X'')$ is called phase delay δ. The phase is delayed if $\delta>0$ and advanced if $\delta<0$. Moreover, we can obtain the map $g:S^1\to S^1$ defined as

$$g:\phi(X)\mapsto\phi(X'') \quad \text{or} \quad \phi(X'')=g(\phi(X))=\phi(X)-\delta. \tag{4.3}$$

The graph of the map g is called *the phase transition curve* (PTC).

In order to calculate the delay, one should take a limit $t\to\infty$. Practically, however, it is possible to approximate the delay by replacing the limit operation in Eq. (4.2) by

$$||\Phi(X',t)-\Phi(\tilde{X},t)||<\varepsilon, \tag{4.4}$$

where X' is a perturbed point from $X\in\gamma$ by the stimulus, $\tilde{X}\in\gamma$, and ε is a small positive number that we determine. This means that we identify X' with $\tilde{X}\in\gamma$ within a finite time and assume that these two points behave identically in their future. (See Fig. 6.) Let t_p be the minimum time needed for the perturbed point X' to satisfy the above inequality (4.4) for some point $\tilde{X}\in\gamma$ and t_n be the time elapsed for $X\in\gamma$ to arrive at $\Phi(\tilde{X},t_p)$ along γ. Since $X'\in W^s(\tilde{X})$ by the assumption, $\delta=\phi(X)-\phi(\tilde{X})$. Moreover, since $\Phi(X',t_p)=\Phi(\tilde{X},t_p)$ and $\Phi(X,t_n)=\Phi(\tilde{X},t_p)$ by the assumption, $\delta(X,A,\varepsilon)$ can be calculated as

$$\delta(X,A,\varepsilon)=t_p-t_n. \tag{4.5}$$

The notation $\delta(X,A,\varepsilon)$ accounts for the fact that the phase shift δ is a function of the state point when the stimulus is applied, the intensity of the stimulus, and the precision of the approximation. By numerical simulations, we obtain the values of t_p, t_n, and then $\phi(\tilde{X})$, the approximation of the PTC, as

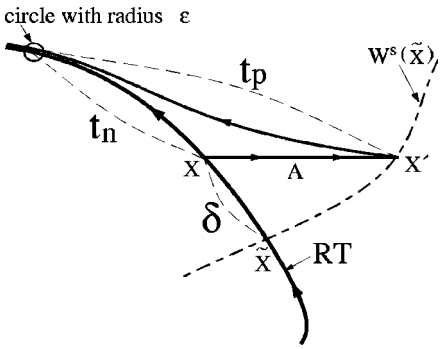

FIG. 6. Schematic diagram for the effect of a perturbation. (See the text for details.) The units of the axes are arbitrary.

$$\phi(\tilde{X})=\phi(X)-\delta(X,A,\varepsilon). \tag{4.6}$$

Let us consider the case when the second stimulus is applied a time T after the first one. If T is larger than t_p, then we can consider that the state point when the second stimulus is applied is on the limit cycle γ with precision better than ε. The phase of the state point just before the second stimulus, denoted by ϕ', will be

$$\phi'=\phi(\tilde{X})+T=\phi-\delta(X,A,\varepsilon)+T \pmod N, \tag{4.7}$$

where ϕ represents $\phi(X)$. We call the map between ϕ and ϕ' *the one-dimensional map* (1D); $\phi'=f(\phi,T)$.

As observed in Sec. II, any trajectory of the excitable FHN equations with a small spiral approaches the RT. Using the RT, we extend the definitions of phase and 1D maps to the excitable model with a small spiral. We take the trajectory toward the equilibrium starting from the datum point as the RT [Fig. 2(a)]. The datum point is on the right-hand branch of the x nullcline and its y value is the same as that of the equilibrium point. We define the phase of a state point on the RT, instead of the limit cycle, as the time elapsed to arrive there from the datum point along the RT. This RT gives satisfactory results as we will show later. To obtain the delay function δ and then 1D maps approximately, we use the same practical procedure as for the limit cycle oscillator [24].

When the equilibrium point is a less attractive focus, trajectories converge to the equilibrium along the spiral, which winds around the equilibrium point with relatively large radius. Even in this case, we take one of the winding trajectories as the RT as shown in Fig. 2(b). The definition of the system's phase along the RT needs to be adapted to the fact that the winding trajectory near the equilibrium is not as attractive as either the limit cycle or the slow manifold of the excitable FHN equations with a small spiral [25]. This means that state points that are not on the RT do not asymptotically approach it, but create their own spiral toward the equilibrium.

Rabinovitch *et al.* [18] showed that using the same definition of phase, one can obtain δ by the following modification: (i) Let P_1 be the state point on the RT when a single

pulse stimulus is applied and P_1' be the perturbed point. The trajectory starting from P_1' creates its own spiral winding around the equilibrium that converges to the equilibrium. Let P_2 be the first y-minimum point (i.e., bottom of the spiral) starting from the perturbed point P_1' and P_3 be the closest y-minimum point to P_2 on the RT. (ii) The time elapsed to reach P_2 from the perturbed point P_1' provides t_p in Eq. (4.5). (iii) The time elapsed to reach P_3 from P_1 along the RT provides t_n in Eq. (4.5).

This procedure is an approximation with the assumption that P_2 and P_3 behave identically in their future, although there always exists some distance between them. If we accept this approximation, the procedure to obtain the delay function δ is the same as that for the oscillatory or excitable with small spiral. This procedure makes the error relatively small since the phase of the state point that is not on the RT is evaluated on the one-dimensional curve, constituted by the bottom of the spiral RT.

In the continuous 1D maps, we assumed that after each perturbation, the state point moved toward either the limit cycle or the RT. This assumption is valid when the system is monostable, i.e., it has a unique stable equilibrium point or a unique stable limit cycle. In the region of bistability, however, there are amplitude ranges for which some points on the limit cycle are kicked into the basin of attraction of the stable equilibrium point. For such phases, gaps appear in the corresponding 1D maps as the next phase is not defined [22]. We have constructed 1D maps in the bistable regimes and analyzed their iterations. However, in the following, we will not discuss in detail the influence of these gaps on the dynamics of the system. This is due to the fact that they affect only small regions in the 2BDs of the system and in this work we are more interested in the changes in the global organization of the 2BDs.

B. Dynamics of the one-dimensional maps

The dynamics of the periodically stimulated FHN equations can be described by the phases when the stimulus is applied to the system. For any given initial phase ϕ_0 at which the first stimulus is applied to the system, it is possible to define the subsequent sequence $\{\phi_n\}$ inductively using the 1D map $f(\phi,T)$:

$$\phi_n = f(\phi_{n-1},T) = f^2(\phi_{n-2},T) = \cdots = f^n(\phi_0,T). \tag{4.8}$$

The phase sequence $\{\phi_n\}$ are plotted on the one-dimensional map for an arbitrary but fixed input period T. We call the locus $\{\phi_n\}$ the orbit of the map. If $\phi_{m+p}=\phi_m$ and $\phi_{m+k} \neq \phi_m$ for $1 \leqslant k < p$ with k, m, and p being positive integers, $\{\phi_n\}$ is a periodic sequence of period p. A periodic sequence $\{\phi_k\}_{k=0}^{p-1}$ of period p is stable if the following equation holds:

$$\left|\frac{\partial f^p}{\partial \phi}(\phi_0)\right| = \prod_{j=0}^{p-1}\left|\frac{\partial f}{\partial \phi}(\phi_j)\right| < 1. \tag{4.9}$$

Figure 7 shows examples of the 1D map. Figures 7(d) and 7(f) are the 1D circle maps for the oscillatory model. The maps in Figs. 7(d) and 7(f) first increase monotonically, then decrease steeply, and then increase again gradually. Figure 7(d) displays a period-2 orbit and Fig. 7(f) a chaotic response. The locking ratio of periodically stimulated oscillatory FHN equations defined in Sec. III can be obtained from the circle map using the rotation number ρ [11]. To this end, we use the map f defined in Eq. (4.7) without taking modulo N. Let us call this map $\overline{f}$ for the moment. Let $\Delta\phi_n$ be the phase difference between ϕ_{n-1} and $\overline{f}(\phi_{n-1},T)$; then the rotation number ρ is defined as

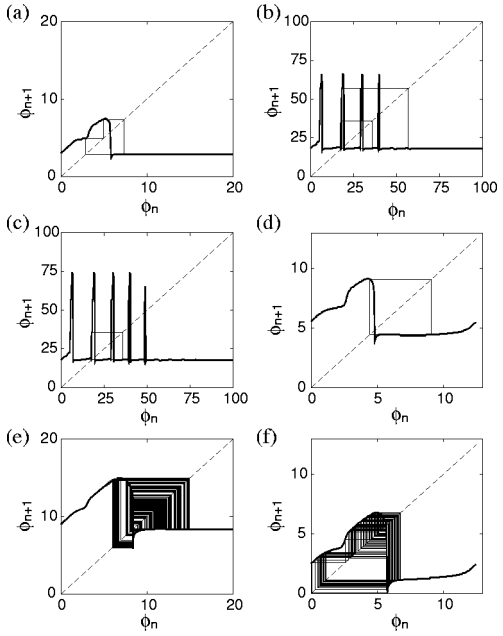

FIG. 7. Examples of the one-dimensional map and the corresponding orbit for the FHN equations. The parameter values of (a)–(f) correspond to the dynamics in Figs. 4(a)–4(f), respectively. The units of the axes are arbitrary.

$$\rho = \lim_{j\to\infty}\frac{\sum_{n=1}^{j}\Delta\phi_n}{j}. \tag{4.10}$$

If $\{\phi_n\}$ is a periodic orbit of period p with rotation number $\rho=q/p$, then we say that the response is $p{:}q$ phase locking, where q is a positive integer

$$q = \sum_{n=1}^{p}\Delta\phi_n. \tag{4.11}$$

For example, Fig. 7(d) shows the 2:3 phase locking response ($\rho=1.5$). If $\{\phi_n\}$ is asymptotically aperiodic, then ρ is irrational. Indeed, ρ is an irrational number practically in Fig. 7(f).

Figures 7(a) and 7(e) are the cases for an excitable model with a small spiral. Since the RT of the excitable model is not a closed cycle topologically, the corresponding map is not a circle map. Indeed, the domain of definition and the range of the map are $[0,\infty)$ in this case. Nevertheless, the shape of the map is similar to the oscillatory one, except the long lasting flat portion on the right-hand side of the map. The steep negative slope portion of the map separates the monotonically increasing curve on the left from the flat portion on the right. It reflects the threshold behavior of the

membrane model. We denote the phase of the point with the steepest negative slope as ϕ_h. If the stimulus is applied at the phase above ϕ_h, the membrane model fires. If not, the model does not fire. We denote the response to the inputs by the symbols 1 (firing) if the orbit of the map touches the flat portion, and 0 (nonfiring) otherwise. More precisely, we assign the symbols to the sequence $\{\phi_n\}$ as

$$0 \quad \text{for} \quad \phi_n \in [0,\phi_h],$$

$$1 \quad \text{for} \quad \phi_n > \phi_h. \tag{4.12}$$

For example, the sequence $\{\phi_n\}$, except for its transient in Fig. 7(a), is symbolized by 100100 . . . . If $\{\phi_n\}$ is eventually periodic with period p except for its transient and the number of 1 within the p successive symbols is q, then we say that the response is $p:q$ phase locking. The locking ratio obtained from this definition practically coincides with that in Sec. III. For example, Fig. 7(a) shows the 3:1 phase locking response. In Fig. 7(e) the response is practically chaotic.

Figures 7(b) and 7(c) are the cases for the excitable model with a big spiral. The 1D map in this case possesses several peaks. The map is almost flat between these peaks. As in the map for the excitable model with a small spiral [Fig. 7(a)], the map is defined for $\phi \in [0,\infty)$. We symbolize the orbit of the map in a similar way to the excitable model with a small spiral. We divide the map into the flat portions and the others. Let $d_k (k=1,\ldots,h)$ be the phase of the steepest negative slope portion of the map for each kth peak, $e_k (k=1,\ldots,h)$ the phase where the map begins to increase steeply for each kth peak, and h the number of peaks. We assign the symbols to the sequence $\{\phi_n\}$ as

$$0 \quad \text{for} \quad \phi_n \in [0,d_1] \quad \text{or} \quad \in (e_k,d_k] \quad (k=1,\ldots,h),$$

$$1 \quad \text{for} \quad \phi_n \in (d_k,e_{k+1}] \quad (k=1,\ldots,h-1) \quad \text{or} \quad \phi_n > d_h. \tag{4.13}$$

Note that Eq. (4.12) (for a small spiral) corresponds to Eq. (4.13) (for a big spiral) with $h=1$. For example, Figs. 7(b) and 7(c) show the 4:2 and 2:1 phase locking responses, respectively. Although the z value is the same for Figs. 7(b) and 7(c), the number of peaks in the maps is different since the parameter values of the stimulus (T,A) are different. In general, when z increases, the number of peaks in the maps increases. For a fixed z and (T,A), the interpeak interval gradually decreases as ϕ increases. For ϕ above some value, the peak disappears suddenly and the remaining portion is almost flat with small oscillations. As the z value becomes close to the double cycle bifurcation point, the number of the peaks becomes larger (tend to infinity) and eventually the 1D map may coincide with the circle map for the oscillatory model.

We can conclude that the shape of the 1D map changes continuously along the transition. To better understand this continuity, we propose a simple model that mimics the topological behavior of the maps for the excitable-oscillatory FHN equations in the next section.

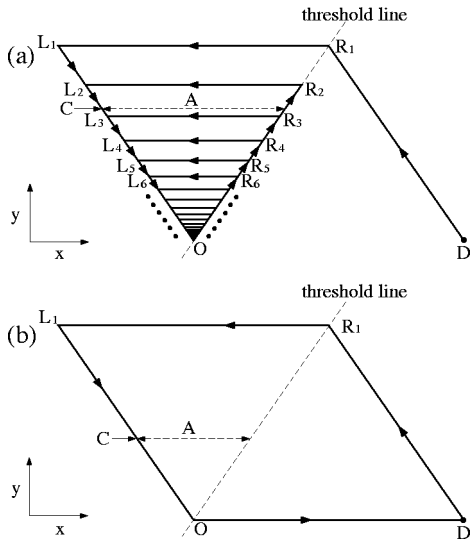

FIG. 8. (a) RT of the simple membrane model in the x-y plane in the case for $0 \leqslant r < 1$. (b) RT of the simple membrane model in the x-y plane in the case for $r=1$, which corresponds to the limit cycle of the FHN equations. The units of the parameter r and the axes are arbitrary.

V. SIMPLE MODEL

In the preceding section we observed that the bifurcation structure of the periodically stimulated FHN equations changes continuously along the transition. In this section we introduce a simple model to understand clearly how the shape of the 1D map changes continuously along the transition and how it affects the bifurcation structure of the map.

First, we construct a simple model that reflects essential dynamics of the forced FHN equations. The model is not described by differential equations. We just assimilate the system's state on the RT of the FHN equations. We simplify the RT of the FHN equations in the x-y phase plane as shown in Fig. 8. It mimics the spiral-shaped RT of the FHN equations and starts from the datum point D, which corresponds to the peak of an action potential of the FHN equations. The terminal point corresponds to the equilibrium of the FHN equations. We parametrize the RT by one parameter r and assume that the converging rate of the winding trajectory to the terminal depends on the parameter r. The parameter r corresponds to the parameter z in the FHN equations. When $r=0$ or $r=1$, the RT does not show a spiral. We associate the former with the excitable FHN equations without a spiral and the latter with the oscillatory limit cycle.

The state point on the simplified RT moves as follows:

$$D \to R_1 \to L_1 \to O \quad \text{1st round},$$

$$O \to R_2 \to L_2 \to O \quad \text{2nd round},$$

$$\vdots \qquad \vdots$$

$$O \to R_m \to L_m \to O \quad \text{mth round},$$

$$\vdots \qquad \vdots$$

The point O is set to the origin and the datum point $D=(1,0)$. Let $L_m=(a_m,b_m)$ and $R_m=(c_m,b_m)(m=1,2,3,\ldots)$ be the coordinates of the points depicted in Fig.

8. We set $R_1=(1/2,\sqrt{3}/2)$ and $L_1=(-1/2,\sqrt{3}/2)$ and the subsequent points are defined as

$$a_m=-\frac{1}{2}r^{m-1},\quad b_m=\frac{\sqrt{3}}{2}r^{m-1},\quad c_m=\frac{1}{2}r^{m-1}$$

$$(m=1,2,3,\ldots). \tag{5.1}$$

If $0\leqslant r<1$, then R_m and L_m converge to the origin. If $r=1$, we assume that the RT changes its shape abruptly to the closed orbit corresponding to the limit cycle defined as $D\rightarrow R_1\rightarrow L_1\rightarrow O\rightarrow D$. See Fig. 8(b).

The following are the assumptions for the model.

(a) The moving velocity of the state point along the line DR_1 is a function of the y-coordinate value of the state point as

$$\dot{y}=(y-b_1-\eta)/\lambda\quad(\lambda=-1.5,\quad\eta=0.01). \tag{5.2}$$

The velocity decreases linearly as y approaches R_1.

(b) The state point jumps from R_m to L_m instantaneously for each mth round ($m=1,2,\ldots$) (from R_1 to L_1 and from O to D in the case $r=1$).

(c) The moving velocity of the state point along the line L_1O is a function of the y-coordinate value of the state point as

$$\dot{y}=(y+\eta)/\lambda. \tag{5.3}$$

It decreases linearly as y approaches the origin. On OR_m in the mth round along the line OR_1, the velocity increases linearly with the same rate as in Eq. (5.3) for L_1O. When $r=0$, the state point reaches the point O within a finite time from D. We assume that the state point remains at the point O.

(d) The state point is displaced horizontally by an amount $A>0$ if it is perturbed by a stimulus. The perturbed point returns to the RT horizontally and instantaneously. If the perturbed point from the L_1O branch is above OR_1 (corresponding to the threshold), it jumps to the right-hand branch of the RT horizontally and instantaneously (an action potential generation). If the perturbed point is below the threshold and it is between the mth and the $(m+1)$th rounds of the RT, then it instantaneously returns to the RT in the mth round.

From these assumptions we can obtain several quantities needed to construct the 1D map. The necessary time $t^D_{1\rightarrow 2}$ from (x_1,y_1) to (x_2,y_2), when these two points are on the line DR_1, is obtained from assumption (a) as

$$t^D_{1\rightarrow 2}=\lambda\ln\left(\frac{b_1+\eta-y_2}{b_1+\eta-y_1}\right)\quad(0\leqslant y_1\leqslant y_2\leqslant b_1). \tag{5.4}$$

The necessary time $t^L_{1\rightarrow 2}$ from (x_1,y_1) to (x_2,y_2), when these two points are on the line L_1O and in the same mth round, is obtained from assumption (c) as

$$t^L_{1\rightarrow 2}=\lambda\ln\left(\frac{y_2+\eta}{y_1+\eta}\right)\quad(0\leqslant y_2\leqslant y_1\leqslant b_m). \tag{5.5}$$

The necessary time $t^R_{1\rightarrow 2}$ from (x_1,y_1) to (x_2,y_2), when these two points are on the line OR_1 and in the same mth round, is obtained from assumption (c) as

$$t^R_{1\rightarrow 2}=\lambda\ln\left(\frac{y_1+\eta}{y_2+\eta}\right)\quad(0\leqslant y_1\leqslant y_2\leqslant b_m). \tag{5.6}$$

The necessary time to reach the end of the mth round from the datum point D in the case $0\leqslant r<1$, denoted by $\tau(m)$, is obtained from assumptions (a)–(c) as

$$\tau(m)=2\lambda\sum_{i=1}^{m}\ln\left(\frac{\eta}{b_i+\eta}\right). \tag{5.7}$$

The natural period N of the oscillation in the case $r=1$ is

$$N=2\lambda\ln\left(\frac{\eta}{b_1+\eta}\right). \tag{5.8}$$

We define the phase of the state point on the RT as the time elapsed from the datum point D along the RT in the same way as for the FHN equations. When $r=1$ we take modulo N. For instance, the phase of the point $L_k=(a_k,b_k)$ in the mth round, denoted by $p(m,k)$, is obtained using Eqs. (5.5)–(5.7) as

$$p(m,k)=\tau(m-1)+\lambda\ln\left(\frac{\eta(b_k+\eta)}{(b_m+\eta)^2}\right). \tag{5.9}$$

There exists a critical point $C=(x_c,y_c)$ on the line L_1O that separates firing from nonfiring when a stimulus with intensity A is applied. Since the horizontal distance between C and the line OR_1 is equal to A, $C=(-A/2,\sqrt{3}A/2)$. When the point C is between L_{m_e} and L_{m_e+1} for some positive integer m_e, the trajectory starting from the datum point D passes through C for each round until the m_eth round. The phase of C depends on the round number of the trajectory. For $0\leqslant r<1$, the phase of the point C in the mth round, denoted by $\theta(m)$ for $m\leqslant m_e$, is

$$\theta(m)=\tau(m-1)+\lambda\ln\left(\frac{\eta(\sqrt{3}A+2\eta)}{2(b_m+\eta)^2}\right). \tag{5.10}$$

Thus the stimulus with intensity A may or may not induce a firing depending on its phase when the system's phase is less than $\theta(m_e)$. If the phase is above $\theta(m_e)$, then the stimulus always induces firing. When $r=1$, the phase of the point C, denoted by θ, is uniquely determined as

$$\theta=\lambda\ln\left(\frac{\eta(\sqrt{3}A+2\eta)}{2(b_1+\eta)^2}\right). \tag{5.11}$$

The 1D map $f(\phi,T)$ is defined in the same way as the FHN equations (4.7) and (4.8). In this case, we can calculate the equation of the map $f(\phi,T)$ analytically. Let ϕ_n and ϕ_{n+1} be the phase of the system when the nth and the $(n+1)$th stimuli are applied, respectively. Then $f(\phi,T)$ in the case for $0\leqslant r<1$ is

$$\phi_{n+1}=\phi_n+T \quad \text{for } 0\leqslant\phi_n\leqslant\theta(1), \quad 0\leqslant\phi_n<p(1,1), \tag{5.12}$$

$$\phi_{n+1}=\phi_n+\tau(k-1)+2\lambda\ln\left(\frac{b_1+\eta}{b_k+\eta}\right)+T \quad \text{for } 0\leqslant\phi_n\leqslant\theta(1), \quad p(1,k)\leqslant\phi_n<p(1,k+1) \quad (k=1,2,3,\ldots), \tag{5.13}$$

$$\phi_{n+1}=\lambda\ln\left(\frac{-(b_1+\eta)^2\exp(\phi_n/\lambda)+\eta(b_1+2\eta)}{\eta(b_1+\eta)}\right)+T \quad \text{for } \theta(1)<\phi_n<\tau(1), \tag{5.14}$$

$$\phi_{n+1}=\lambda\ln\left(\frac{-\eta\exp[-\{\phi_n-\tau(m-1)\}/\lambda]+b_1+2\eta}{b_1+\eta}\right)+T \quad \text{for } \tau(m-1)\leqslant\phi_n<p(m,m) \quad (m=2,3,4,\ldots), \tag{5.15}$$

$$\phi_{n+1}=\phi_n+\tau(k-1)-\tau(m-1)+2\lambda\ln\left(\frac{b_m+\eta}{b_k+\eta}\right)+T \quad \text{for } p(m,m)\leqslant\phi_n\leqslant\theta(m),$$

$$p(m,k)\leqslant\phi_n<p(m,k+1) \quad (m=2,\ldots,m_e;\ k=m,m+1,\ldots), \tag{5.16}$$

$$\phi_{n+1}=\lambda\ln\left(\frac{-(b_m+\eta)^2\exp[\{\phi_n-\tau(m-1)\}/\lambda]+\eta(b_1+2\eta)}{\eta(b_1+\eta)}\right)+T \quad \text{for } \theta(m)<\phi_n<\tau(m) \quad (m=2,3,\ldots). \tag{5.17}$$

The map $f(\phi,T)$ in the case for $r=1$ is

$$\phi_{n+1}=\phi_n+T(\text{mod } N) \quad \text{for } 0\leqslant\phi_n\leqslant\theta, \tag{5.18}$$

$$\phi_{n+1}=\lambda\ln\left(\frac{-(b_1+\eta)^2\exp(\phi_n/\lambda)+\eta(b_1+2\eta)}{\eta(b_1+\eta)}\right)+T \quad (\text{mod } N) \quad \text{for } \theta<\phi_n<N. \tag{5.19}$$

Figure 9 exemplifies the 1D maps of the simple model. The simple model behaves as an excitable membrane model with a small spiral in Figs. 9(a) and 9(e) ($r=0.0001$), an excitable membrane with a big spiral in Figs. 9(b) and 9(c) ($r=0.5$), and as an oscillatory membrane in Figs. 9(d) and 9(f) ($r=1$). As in Fig. 7 for the FHN equations, the shape of the maps in Figs. 9(a) and 9(d) are similar to each other, although the latter is a circle map and the former is not.

Consider the case $0\leqslant r<1$ when the simple model behaves as an excitable membrane. Using Fig. 9(b) as an example, let us illustrate the shape of the map and how the formulation of the map [Eqs. (5.12)–(5.17)] is obtained. Since $A=0.06$ in Fig. 9(b), the point C is located between L_5 and L_6. As defined above, m_e denotes the final round number until which the RT passes through C. m_e can be obtained as the maximum value of m that satisfies $y_c<b_m$. Hence the value of m_e in this case is 5. We start the illustration from smaller phases for the first round ($m=1$) on the RT where a stimulus is applied. In the following, we use ''the stimulus phase ϕ_s'' and ''the perturbed phase ϕ_p'' to denote the phase where the stimulus is applied and the phase of the state on the RT to which the perturbed point returns just after the stimulation, respectively. If the nth stimulus phase is ϕ_s, the $(n+1)$th stimulus phase will be ϕ_p+T where T is the interstimulus interval.

The formulation of the map for the stimulus phase less than $\tau(1)$ (i.e., until the end of the first round) is as follows.

(i) As shown in Fig. 9(b), $f(\phi,T)$ is a straight line with slope 1 for early ϕ in $[0,p(1,1))$ as explained in the following. Until the stimulus phase reaches $p(1,1)$ (i.e., the state point is located between D and R_1), the state point is always above the threshold line, and the perturbed point returns in-

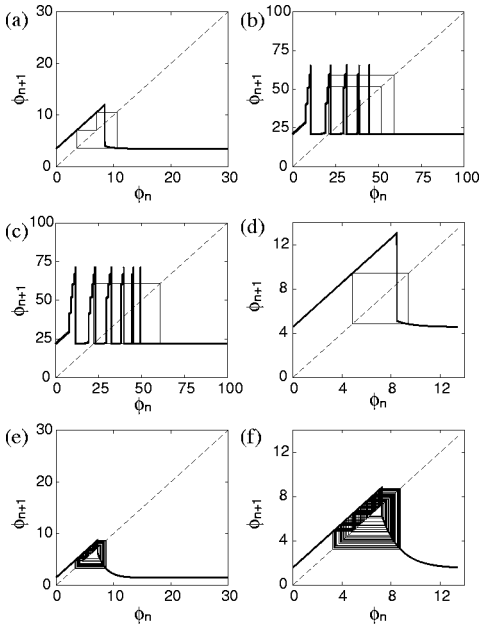

FIG. 9. Examples of the one-dimensional map and the corresponding orbit for the simple model. (a) $r=0.0001$ (excitable with a small spiral), $A=0.3$, and $T=3.5$, 3:1 phase locking response; (b) $r=0.5$ (excitable with a big spiral), $A=0.06$, and $T=21.1$, 4:2 phase locking response; (c) $r=0.5$ (excitable with a big spiral), $A=0.03$, and $T=22.0$, 2:1 phase locking response; (d) $r=1.0$ (oscillatory with a stable limit cycle), $A=0.3$, and $T=18.0$, 2:3 phase locking response; (e) $r=0.0001$ (excitable with a small spiral), $A=0.7$,$T=1.5$, chaotic response; and (f) $r=1.0$ (oscillatory with a stable limit cycle), $A=0.7$, and $T=15.0$, chaotic response. The units of all parameters and axes are arbitrary.

stantaneously to the same point as before the perturbation. Thus $\phi_p=\phi_s$, leading to Eq. (5.12).

(ii) $f(\phi,T)$ is a straight line with slope 1 for $\phi \in (p(1,1),p(1,2))$ and then it increases discontinuously at $p(1,2)$ followed by the straight line with slope 1 for $\phi \in (p(1,2),p(1,3))$. $f(\phi,T)$ increases discontinuously again at $p(1,k)(k=3,\ldots,m_e)$ and each discontinuity is followed by the straight line with slope 1 for $\phi \in (p(1,k),p(1,k+1))(k=3,\ldots,m_e-1)$ and for $\phi \in (p(1,m_e),\theta(1))$. This process with several k generates the first peak at $\phi=\theta(1)$. This is explained as follows. The stimulus phase between $p(1,k)$ and $p(1,k+1)(k=1,\ldots,m_e)$, as long as it is less than $\theta(1)$ (i.e., the state point between L_1 and L_2, L_2 and L_3, L_3 and L_4, L_4 and L_5, and L_5 and C in the first round in this example), does not lead to a firing and the perturbed point returns to the same point as before the perturbation on the line L_1O in the kth round by assumption (d). As the stimulus phase ϕ_s is close to $\theta(1)$, the perturbed point returns to the line L_1O with higher value of k (further inside the spiral), leading to a higher value of the phase ϕ_p after the stimulus. Since the round number of the returned point is constant for $\phi \in (p(1,k),p(1,k+1))$ $(k=1,\ldots,m_e-1)$ for each k and for $\phi \in (p(1,m_e),\theta(1))$, $f(\phi,T)$ is a straight line with slope 1 in each interval as in (i). Thus we obtain Eq. (5.13). Let $L_k(-)$ and $L_k(+)$ be the points infinitesimally above and below L_k on the RT, respectively. The perturbed point from $L_k(-)$ returned in the $(k-1)$th round. Thus the perturbed phase is $p(k-1,k)(k=2,\ldots,m_e)$. The perturbed point from $L_k(+)$ returned in the kth round. Thus the perturbed phase is $p(k,k)(k=2,\ldots,m_e)$. Therefore, $f(\phi,T)$ jumps upward discontinuously at each $p(1,k)(k=2,\ldots,m_e)$ by

$$p(k,k)-p(k-1,k)=2\lambda\ln\left(\frac{\eta}{b_k+\eta}\right). \tag{5.20}$$

(iii) $f(\phi,T)$ jumps downward discontinuously at $\theta(1)$ (right after the first peak) and then it decreases further, followed by the almost flat portion for $\phi \in (\theta(1),\tau(1))$. The stimulus phase greater than $\theta(1)$ and less than $\tau(1)$ (i.e., the state point between C and O in the first round) always leads to a firing and the perturbed state point is transferred to the line DR_1 horizontally by assumption (d). Since the perturbed phase changes suddenly at $\theta(1)$ and the phase of the state point on the line DR_1 is small, ϕ_p or $f(\phi,T)$ decreases discontinuously at $\theta(1)$. The phase ϕ_s of the state point with its y coordinate on the line L_1O in the first round is expressed as

$$\phi_s=\lambda\ln\left(\frac{\eta(y+\eta)}{(b_1+\eta)^2}\right). \tag{5.21}$$

Since the y coordinates of the point when the stimulus is applied and when the perturbed point returns just after the stimulation are the same by assumption (d), the phase ϕ_p on the line DR_1 is, by assumption (a),

$$\phi_p=\lambda\ln\left(\frac{-y+b_1+\eta}{b_1+\eta}\right). \tag{5.22}$$

By eliminating y from Eqs. (5.21) and (5.22), we obtain the relationship between ϕ_s and ϕ_p and then we have Eq. (5.14). Since the state point moves slowly near the point O, $\phi_s \in (\theta(1),\tau(1))$ spans a relatively wide interval. On the other hand, since the state point moves relatively fast near the point D, ϕ_p in this range changes little as ϕ_s changes. Thus the map in this range is almost flat. (See [15] for a similar argument.)

The formulation of the map in the second and higher rounds is as follows.

(iv) $f(\phi,T)$ is still in the almost flat portion with the relatively small value for $\phi \in (\tau(1),p(2,2))$. The stimulus phase greater than $\tau(1)$ and less than $p(2,2)$ (i.e., the state point between O and R_2 in the second round) always leads to a firing and the perturbed state point is transferred to the line DR_1 horizontally. In a similar way as in (iii), the relationship between the phase ϕ_s of the state point with its y coordinate on the line OR_1 in the second round is

$$\phi_s=\tau(1)-\lambda\ln\left(\frac{y+\eta}{\eta}\right) \tag{5.23}$$

and ϕ_p is as in Eq. (5.22). Thus we obtain the relationship between ϕ_s and ϕ_p for this range in the second round as in Eq. (5.15) with $m=2$. As in (iii), $(\tau(1),p(2,2))$ spans a relatively wide interval and $f(\phi,T)$ takes a small value and forms almost flat portion against ϕ.

(v) $f(\phi,T)$ jumps upward discontinuously at $p(2,2)$ followed by the straight line with slope 1 for $\phi \in (p(2,2),p(2,3))$. $f(\phi,T)$ increases discontinuously again at $p(2,k)(k=3,\ldots,m_e)$ and each discontinuity is followed by the straight line with slope 1 for $\phi \in (p(2,k),p(2,k+1))$ $(k=3,\ldots,m_e-1)$ and $\phi \in (p(2,m_e),\theta(2))$. This process with several k generates the second peak at $\phi=\theta(2)$. In a similar way to (ii) in the first round, we obtain Eq. (5.16) with $m=2$. Each discontinuity at $p(2,k)(k=3,\ldots,m_e)$ is also given by Eq. (5.20).

(vi) $f(\phi,T)$ jumps downward discontinuously at $\theta(2)$ (right after the second peak) and then decreases followed by the almost flat portion for $\phi \in (\theta(2),\tau(2))$. In a similar way to (iii) in the first round, we obtain Eq. (5.17) with $m=2$.

(vii) From the third round until the m_eth round ($m_e=5$ in this example), similar formulations in (iv)–(vi) repeat in this order for each $\phi \in [\tau(m-1),\tau(m))(m=3,\ldots,m_e)$.

(viii) $f(\phi,T)$ changes its shape for $\phi \geqslant \tau(m_e)$. Since the stimulus phase ϕ_s is always above $\theta(m_e)$ (i.e., the y coordinate of the state point is always below that of C), the stimulus always induces a firing. Although it is not easy to see from the Fig. 9(b), the map still has a repetitive structure. From the (m_e+1)th round, similar formulations in (iv) and (vi), i.e., Eqs. (5.15) and (5.17), repeat in this order for each $\phi \in [\tau(m-1),\tau(m))(m=m_e+1,m_e+2,\ldots)$.

In this way, the straight lines with slope 1 with several discontinuities and the almost flat portion alternate for $\phi \in [0,\tau(m_e))$ in the 1D map and $f(\phi,T)$ becomes almost flat with a small-amplitude oscillation for $\phi \in [\tau(m_e),\infty)$. The number of peaks coincides with the value of m_e and increases as the value of r increases or the intensity A decreases. $m_e=1,\tau(m_e)=8.7$, and the map has only one peak in Fig. 9(a) ($r=0.0001$ and $A=0.3$); $m_e=5,\tau(m_e)=42.4$, and the map has five peaks in Fig. 9(b) ($r=0.5$ and $A=0.06$); and $m_e=6,\tau(m_e)=46.3$, and the map has six peaks in Fig. 9(c) ($r=0.5$ and $A=0.03$). The shape of the map is

determined only by the parameters r and A. The period T shifts the map upward or downward without affecting its shape [see Eqs. (5.12)–(5.17) or Eqs. (5.18) and (5.19)].

As the value of r approaches 1, the 1D map eventually gains periodic structure. The discontinuous increase $p(k,k)-p(k-1,k)$ in each peak of the map at each $p(m,k)(m \leqslant m_e)$ was given in Eq. (5.20) and the natural period of the oscillation in the case $r=1$ was given in Eq. (5.8). Since $b_k \to b_1$ as $r \to 1$,

$$p(k,k)-p(k-1,k) \to N \tag{5.24}$$

and the interpeak interval of the map

$$\theta(m+1)-\theta(m)=2\lambda \ln\left(\frac{\eta}{b_{m+1}+\eta}\right) \to N, \tag{5.25}$$

where $m<m_e$ as $r \to 1$. Hence, by taking modulo N for both the domain of definition and the range of the map, the map becomes a circle map. This indicates that the map changes continuously when the model dynamics changes from excitability to oscillation. However, strictly speaking, this observation does not hold rigorously since we assume that the shape of the RT changes abruptly at $r=1$. The map for ϕ smaller than $\tau(1)$ exactly coincides with the map for oscillatory membrane ($r=1$) in Eqs. (5.18) and (5.19), but the map for $\phi>\tau(1)$ differs slightly from that for $\phi<\tau(1)$. Note that the map for $r=1$ has complete periodicity with period N in both the domain and the range of the map for $\phi \geqslant \tau(1)$. Since the shape of the RT changes continuously at the bifurcation point between excitable and oscillation in the FHN equations, we can speculate strongly that the 1D map changes continuously at the bifurcation point.

Comparing the 1D map of the FHN equations (Fig. 7) with that of the simple model (Fig. 9), we can see a similarity. Hence the illustration for continuous change of the simple map shape can be applicable for the FHN equations.

As in Eqs. (4.10), (4.12), and (4.13) for the FHN equations, we symbolize the map's dynamics by 1 (firing) if the orbit of the map touches the flat portion and 0 (nonfiring) otherwise. More precisely, we assign the symbols to the sequence $\{\phi_n\}$ as follows: For $r=0$,

$$0 \quad \text{for} \quad \phi_n \in [0,\theta(1)],$$

$$1 \quad \text{for} \quad \phi_n > \theta(1) \tag{5.26}$$

and for $0<r<1$,

$$0 \quad \text{for} \quad \phi_n \in [0,\theta(1)] \quad \text{or} \quad \phi_n \in (p(m,m),\theta(m)]$$

$$(m=1,\ldots,m_e),$$

$$1 \quad \text{for} \quad \phi_n \in (\theta(m),p(m+1,m+1)]$$

$$(m=1,\ldots,m_e-1) \quad \text{or} \quad \phi_n > \theta(m_e). \tag{5.27}$$

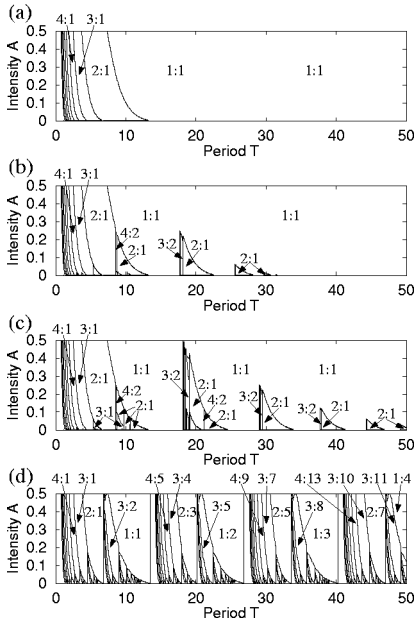

FIG. 10. Two-parameter bifurcation diagrams of the simple model stimulated by periodic pulse trains with several values of the parameter r. The ordinate is the pulse intensity A and the abscissa is the period T. See the caption of Fig. 5 for the illustration of the diagram. The values of the parameter r are (a) $r=0.0001$ (excitable with a small spiral), (b) $r=0.25$ (excitable with a relatively big spiral), (c) $r=0.5$ (excitable with a big spiral), (d) $r=1.0$ (oscillatory with a limit cycle). The units of r and the axes are arbitrary.

For $r=1$, we calculate the rotation number ρ by Eq. (4.10). For instance, Figs. 9(a), 9(b), 9(c), and 9(d) show the 3:1, 4:2, 2:1, and 2:3 phase locking responses, respectively, and Figs. 9(e) and 9(f) show the chaotic responses.

We show how the continuous change of the 1D map relates to the continuous change in the global organization of the bifurcation structure. Figure 10 shows the 2BDs of the simple model for several values of r. The value of the parameter r increases from top [Fig. 10(a)] to bottom [Fig. 10(d)].

Figure 10(a) is the case for r extremely small. In this case, the simple model behaves as an excitable membrane with a small spiral and the corresponding 1D map is like Fig. 9(a). The global structure of Fig. 10(a) is similar to that of Fig. 5(a). It shows wide 1:1 phase locking region for large T since the maps shifted upward largely have a unique stable fixed point on the almost flat portion. As T decreases, a period adding cascade generating p:1 phase lockings takes place. See [14] for more details. There is no 0 response region in this simple model because the distance between point O and the threshold line is 0.

Figures 10(b) and 10(c) are the cases for r relatively large when the simple model behaves as an excitable membrane with a big spiral. In this case, the corresponding 1D maps are like Figs. 9(b) and 9(c). The global structure of Figs. 10(b) and 10(c) is similar to that of Figs. 5(b) and 5(c), respectively.

In these diagrams, phase locking regions with higher periods (mountains and valleys) can be observed in the 1:1

phase locking region. As in the FHN equations, for a fixed r [Figs. 10(b) and 10(c)], the peak height of the mountains becomes lower and the intervalley intervals become shorter as the stimulus period T increases. Moreover as r increases, the height of the mountains becomes higher from Fig. 10(b) to 10(c), and the intervalley intervals become larger. This change can be understood from the dynamics of the 1D maps of the simple model. Let us assume a 1D map that possesses m_e peaks for some fixed r and A. Then the map has m_e almost flat portions between the peaks. The last m_eth almost flat portion spans $[\theta(m_e),\infty)$. Assume that the first almost flat portion of the map intersects with the diagonal for some small T. The intersection point is a stable fixed point of the map and provides 1:1 phase locking region in the 2BD. For increasing T the map just shifts upward and the intersection point moves rightward. When the intersection point reaches $p(2,2)$, the intersection point disappears and the 1:1 phase locking is terminated. Further increasing T, the second almost flat portion intersects with the diagonal and 1:1 phase locking appears again. This process alternates as T increases until $T=\theta(m_e)$ and for $T>\theta(m_e)$ the 1:1 phase locking region persists. Since m_e, the number of peaks in the map, decreases as A increases, the range of T with this alternate structure (i.e., the appearance and disappearance of the 1:1 region) for a fixed A value becomes smaller as A increases. For the same reason, the height of the mountains in the 2BD becomes lower as T increases. Similarly, since m_e increase as r increases, the height of the mountains becomes higher as r increases.

Since the 1D map gains periodicity in the direction of both the domain of definition and the range of the map with period N as r becomes close to 1, the mountains appear periodically with period N in the direction of T and intervalley intervals become close to the natural period of the oscillation N. Eventually, the bifurcation structure gains periodicity for the oscillatory model [$r=1$, Fig. 10(d)].

VI. DISCUSSION

We used FitzHugh-Nagumo equations as a model of neuronal excitations. The model exhibits both an excitation in response to an impulsive current stimulation and a spontaneous oscillation depending on the parameter value z, which reflects the intensity of the constant dc applied to the model. The critical points that separate the excitable from the oscillatory membrane models are the double cycle and the Hopf bifurcations in the model.

In this study we explored the model's dynamics when the membrane model is stimulated periodically by impulsive trains with various periods T and intensities A. As in many other nonlinear systems, the forced model showed $p:q$ phase lockings as well as chaotic dynamics depending on the parameter values (T,A). The dynamics of the model was summarized in the 2BD in (T,A) parameter plane. In particular, we showed that the global organization of the 2BD changes depending on the model's intrinsic parameter z. Despite the drastic change in the system's asymptotic dynamics at the double cycle bifurcation point, the changes in the diagram are a continuous function of the parameter value z.

To see these changes, we defined the appropriate 1D maps f to describe the dynamics of both the oscillatory and the excitable membrane models stimulated by periodic pulse trains. This was done by extending the concept of phase ϕ and isochron utilized for oscillatory systems to excitable systems. A similar method was used in [18]. Different 1D maps approximating Poincaré maps of the periodically stimulated FHN equations have been proposed. Let $X\in\mathbb{R}^2$ be the state point of the FHN equations. All trajectories in the FHN phase plane approach the one-dimensional curve referred to as the reference trajectory. For the oscillatory FHN equations, the RT coincides with the limit cycle. Using the RT, a key point to constructing a 1D map is finding an appropriate one-to-one mapping ϕ that maps each X on the RT to a uniquely determined scalar variable. Different mapping ϕ leads to a different 1D map. Let ϕ_x and ϕ_y be such mappings and $\mathcal{X}=\phi_x(X)$ and $\mathcal{Y}=\phi_y(X)$ be the corresponding scalar variables, respectively. A 1D map is obtained by plotting $\phi(X_{i+1})$ against $\phi(X_i)$, where X_i represents the system's state when the ith stimulus is applied. If $\mathcal{Y}$ is a strictly increasing function of $\mathcal{X}$, then there is a one-to-one relationship between the two [i.e., $\mathcal{Y}=u(\mathcal{X})$ or, equivalently, $\mathcal{X}=u^{-1}(\mathcal{Y})$]. Accordingly, this relationship suggests that corresponding 1D map $f_{\mathcal{Y}}$ is conjugate to $f_{\mathcal{X}}$ in the sense that

$$f_{\mathcal{Y}}=u\circ f_{\mathcal{X}}\circ u^{-1}. \tag{6.1}$$

Thus, once u is determined, a simple geometrical construction allows us to transform $f_{\mathcal{X}}$ to $f_{\mathcal{Y}}$ and vice versa. Using Eq. (6.1), we discuss the relation between f (the 1D map used in this paper) and some other maps. Nomura *et al.* [15] constituted a 1D map for the oscillatory FHN equations using a geometrical angle θ to describe the system's state X on the limit cycle. They measured the angle between the line connecting the unstable equilibrium of the FHN equations to a certain datum point on the limit cycle and the line connecting the former to the point X on the limit cycle. Since the angle θ increases as the time phase ϕ increases, θ is a strictly increasing function of ϕ. Thus their 1D map is conjugate to f. However, their 1D map cannot be extended to the excitable FHN equations with a big spiral since the state point on the spiral-shaped RT cannot be expressed uniquely by the geometrical angle θ, whereas our map f can be extended. Doi and Sato [14] constituted a 1D map for the excitable FHN equations with a small spiral using the membrane potential of the model. This is possible since the membrane potential increases monotonically toward the resting potential from the most hyperpolarized state after every firing (see Fig. 2) and thus, within this range, the state point on the RT and the membrane potential have a one-to-one correspondence. Their 1D map is also conjugate to ours. Since the one-to-one correspondence between the membrane potential and the state point is limited within the range mentioned above, it cannot be extended to the oscillatory or the excitable FHN equations with a big spiral. Kaplan *et al.* [21] computed the area $\mathcal{A}_i$ under the deflection induced by the ith stimulus and showed that plots of the return maps representing $\mathcal{A}_i$ versus $\mathcal{A}_{i+1}$ revealed the characteristics of the response of the membrane to periodic stimulation. In order to compare their method with the one used in this paper, we computed the deflection $\mathcal{A}$ induced by a pulse arriving at a phase ϕ and observed that, except for short phases corresponding to the action potential, $\mathcal{A}$ is a strictly increasing function of ϕ that reveals

that their return maps can be derived from ours and vice versa using Eq. (6.1) for the limited phase. Kaplan *et al.* [21] were interested in the skipping patterns in the response of an excitable cell to a subthreshold periodic stimulation. Therefore, they limited their investigation to small amplitudes and short periods, as skipping was mainly observed in this parameter range. In contrast, we were interested in the response in a wider parameter range, which explains that we obtained 1D maps with a wider variety of shapes (see Fig. 7) than the ones they observed.

In comparison with these three methods exemplified above, the state point on the RT for both the excitable FHN equations with a spiral and the oscillatory FHN equations can be expressed uniquely by the time phase that we used for ϕ in this paper. This advantage allows us to investigate the continuous changes in the 2BD by the continuous changes in the shape of the 1D maps. Along the transition from excitable to oscillatory regimes of the model, the 1D map changes continuously from the multimodal maps to the circle maps. We confirmed this observation analytically by using simple 1D maps that mimic the maps for the forced FHN model.

The continuous changes in 2BDs result from the fact that, despite the discontinuous change that takes place in the global attractor of the unforced system at the double cycle bifurcation, the underlying vector field that governs the dynamics changes continuously with z. This fact can be seen in Fig. 1, which shows that the number of transient spikes generated by the excitable membrane model increases as the stimulus intensity increases toward the double cycle bifurcation point. Let us provide a formal basis for the relation between the continuity of the flow and that of the Arnold tongues. We denote by $\Phi(X,t;z)$ the flow associated with Eq. (2.1); then $\Phi(X,t;z)$ is a continuous function of all its arguments. The dynamics of the periodically forced system can be described by the iterations of the two-dimensional map $F(X,A,T,z)=\wp_A\circ\Phi(X,T;z)$, where $\wp_A$ is the translation of the vector $(A,0)$ [20]. Locking responses correspond to the periodic orbits of the map F. Thus the boundaries of Arnold tongues in the (T,A) parameter plane correspond to singularities of the map F. Typically, these boundaries are saddle-node bifurcations, that is, points X^* such that $F^p(X^*,A^*,T^*,z)=X^*$ and $\det(DF^p_{X^*}-I)=0$. Since these conditions are persistent under small perturbations of the map F and this map depends continuously on the parameter z, we ''expect'' that if such a bifurcation takes place at the parameters A_0^* and T_0^* for some z_0, a similar bifurcation takes place for some A^* and T^* near A_0^* and T_0^* for z near z_0. The above explanation provides further theoretical support for the continuous changes observed in the 2BDs as z was varied. A detailed analysis of the bifurcation of the map F will be performed in the future to complement the above statement.

A further observation of the continuous changes in the 2BD is that the location of the chaotic regions in the 2BD may change continuously along the transition, although detailed investigations are needed to clarify this. Let us make this statement clear.

To this end, first we summarize the dynamics of circle maps. Circle maps can be divided into two classes according to their topological properties. One is a monotonically increasing map and the other is a nonmonotonic one. The former case is relatively well analyzed [11] and the maps show only periodic and quasiperiodic dynamics. Stable fixed points or periodic orbits with different periods cannot coexist in the map. In the latter case, the nonmonotonic circle maps can exhibit complex dynamics including multistability and chaos as well as periodic dynamics. In cases of forced limit cycle oscillators, in general, the monotonically increasing maps are obtained for weak stimulations (lower intensities) and the nonmonotonic ones for higher intensities. The former is referred to as a type 1 map and the latter as type 0 [3,26]. This means that complex dynamics regions, including chaotic regions, in the 2BD will be observed for a relatively high stimulus intensity region, especially near the boundary intensity separating one type from the other. This was confirmed in our simulations, although several complex dynamics were observed even for small intensity regions (this is because the forced dynamics of the model cannot be described completely by 1D maps, i.e., limitation of the one-dimensional approximation of the Poincaré maps).

Second, we summarize the bifurcation structure of periodically forced excitable membranes and compare it to that of the circle maps using Fig. 5. Figure 5(a) is a typical 2BD of forced excitable membranes. In these diagrams, the dominant regions are 1:1, 2:1, and 3:1 phase locking regions and the subdominant regions with $(p+p'):(q+q')$ were observed between adjacent dominant regions with $p:q$ and $p':q'$. Between these subdominant regions, several chaotic regions were observed. In contrast to the circle map cases, these complex dynamics regions were observed even in the relatively low stimulus intensity regions, for example, along the boundary that separates the 0 response region from the other regions. In our simulations, various kinds of dynamics including chaotic ones were unfolded from this boundary when the parameter z increased toward the double cycle bifurcation point. This suggests that the chaotic regions observed for lower z along the boundary may increase as z increases and connect with the chaotic regions in the higher intensity regions generated by the type 0 circle maps.

Although we did not report them in this paper, we also analyzed continuous changes of Arnold tongues in the (T,A) parameter plane for a piecewise linear version of the FHN equations, in particular at the singular limit $c\to\infty$ [27]. In this case, the transition from an excitable to an oscillatory membrane when the intrinsic parameter z value is varied is neither a Hopf nor a double cycle bifurcation, but at the onset of the appearance of the limit cycle oscillation, the period of the oscillation is infinity. Therefore, as z decreases from the oscillatory regime toward the transition point, the periodic structure of the 2BD is stretched in the period T direction and eventually the diagram with period infinity coincides with that for the excitable medium.

Finally, we conclude the paper with the following statement: When an appropriate control parameter of the neuronal membrane model changes its value, the model's behavior changes from quiescent to sustained oscillation. One can interpret this as the model's dynamics representing the intensity of the control parameter in an all-or-none fashion. That is, for the parameter range within the quiescent state, no spike (i.e., no information about the control parameter value) is transmitted by the membrane. If the state of the model is

perturbed, by periodic excitatory inputs in our case, the model generates spike sequences with various temporal structures that reflect the control parameter value. That is, the temporal structures change as the control parameter value changes and they can be interpreted as a representation of the control parameter value.

ACKNOWLEDGMENTS

This work was partially supported by Grants-in-Aid for Scientific Research from the Japanese Ministry of Education, Science and Culture [Grants Nos. (2)09268224 and (c)(2) 09680853].

[1] D.H. Perkel, J.H. Schulman, T.H. Bullock, G.P. Moore, and J.P. Segundo, Science **145**, 61 (1964); D.H. Perkel and T.H. Bullock, Neural Coding. Neurosci. Res. Program Bull. **6**, 221 (1968).

[2] L. Glass and M.E. Josephson, Phys. Rev. Lett. **75**, 2059 (1995).

[3] A.T. Winfree, *The Geometry of Biological Time* (Springer-Verlag, Berlin, 1980).

[4] A.L. Hodgkin and A.F. Huxley, J. Physiol. (London) **117**, 500 (1952).

[5] R. FitzHugh, Biophys. J. **1**, 445 (1961); J. Nagumo, J. Arimoto, and S. Yoshizawa, Proc. IRE **50**, 2061 (1962).

[6] M.R. Guevara, in *A Chaotic Hierarchy*, edited by G. Baier and M. Klen (World Scientific, Singapore, 1991); G. Matsumoto, *Axonal Excitability—Its Phenomena and Molecular Mechanism* (Maruzen, Tokyo, 1981), Vols. 1 and 2; K. Aihara and G. Matsumoto, Biophys. J. **41**, 87 (1983); J. Rinzel, Fed. Proc. **37**, 2793 (1978).

[7] J. Guckenheimer and P. Holmes, *Nonlinear Oscillations, Dynamical Systems, and Bifurcations of Vector Fields* (Springer-Verlag, New York, 1986), Vol. 42.

[8] J. Rinzel and G.B. Ermentront, in *Methods in Neuronal Modeling: From Synapses to Networks*, edited by C. Koch and I. Segev (MIT Press, Cambridge, MA, 1989), Chap. 5.

[9] L. Glass and M.C. Mackey, J. Math. Biol. **7**, 339 (1979); L. Glass, in *Nonlinear Oscillations in Biology and Chemistry*, edited by H. G. Othmer, Lecture Notes in Biomathematics Vol. 66 (Springer-Verlag, Berlin, 1986), p. 232; R. Mettin, U. Parlitz, and W. Lauterborn, Int. J. Bifurcation Chaos Appl. Sci. Eng. **3**, 1529 (1993).

[10] M.R. Guevara, L. Glass, and A. Shrier, Science **214**, 1350 (1981); J.P. Segundo, E. Altshuler, M. Stiber, and A. Garfinkel, Int. J. Bifurcation Chaos Appl. Sci. Eng. **1**, 549 (1991); S. Ishizuka and H. Hayashi, Brain Res. **723**, 46 (1996); G. Matsumoto, K. Aihara, Y. Hanyu, N. Takahashi, S. Yoshizawa, and J. Nagumo, Phys. Lett. A **123**, 162 (1987).

[11] J.P. Keener and L. Glass, J. Math. Biol. **21**, 175 (1984).

[12] L. Glass, M.R. Guevara, J. Bélair, and A. Shrier, Phys. Rev. A **29**, 1348 (1984); K. Aihara, G. Matsumoto, and G. Ikegaya, J. Theor. Biol. **109**, 249 (1984).

[13] N. Takahashi, Y. Hanyu, T. Musha, R. Kubo, and G. Matsumoto, Physica D **43**, 318 (1990).

[14] S. Sato and S. Doi, Math. Biosci. **112**, 243 (1992); S. Doi and S. Sato, *ibid.* **125**, 229 (1995).

[15] T. Nomura, S. Sato, S. Doi, J.P. Segundo, and M.D. Stiber, Biol. Cybern. **69**, 429 (1993); **72**, 55 (1994); **72**, 93 (1994).

[16] U. Parlitz and W. Lauterborn, Phys. Rev. A **36**, 1428 (1987).

[17] L. Glass and M.C. Mackey, *From Clocks to Chaos: The Rhythms of the Life* (Princeton University Press, Princeton, 1988); J. Nagumo and S. Sato, Kybernetik **10**, 155 (1972); S. Yoshizawa, H. Osada, and J. Nagumo, Biol. Cybern. **45**, 23 (1982).

[18] A. Rabinovitch, R. Thieberger, and M. Friedman, Phys. Rev. E **50**, 1572 (1994).

[19] Indeed, if the parameter value $c \to \infty$, then Eq. (2.1) becomes singular and the vector field away from the cubic-shaped x nullcline in the x direction becomes extremely large compared to that in the y direction. Hence any state point in the phase plane returns quickly to the RT and moves along it toward the equilibrium point.

[20] H. Kawakami, IEEE Trans. Circuits Syst. **CAS-31**, 248 (1984); Y. Ueda and N. Akamatsu, *ibid.* **CAS-28**, 234 (1981).

[21] D.T. Kaplan, J.R. Clay, T. Manning, L. Glass, M.R. Guevara, and A. Shrier, Phys. Rev. Lett. **76**, 4074 (1996), showed that the subthreshold dynamics of squid giant axon as well as those of the FHN equation in response to periodic pulse stimuli with subthreshold intensities are deterministic including phase lockings and chaos. We confirmed this for the 0 response region of the parameter bifurcation diagrams for excitable FHN equations.

[22] G.A. Cecchi, D.L. Gonzalez, M.O. Magnasco, G.B. Mindlin, O. Piro, and A.J. Santillan, Chaos **3**, 51 (1993).

[23] J. Guckenheimer, J. Math. Biol. **1**, 259 (1975).

[24] If the parameter $c \to \infty$ in Eq. (2.1), we can take the value of ε very small since the perturbed point X' returns to the RT immediately after the perturbation.

[25] A critical difference between excitable FHN equations with small and big spirals is as follows. In the former case, the precision of the 1D map approximation can be improved as much as desired if $c \to \infty$. In the latter case, however, there is no such guarantee theoretically. This is because the system with a large enough value of c cannot possess a focal equilibrium, hence no spiral-shaped RT exists. Therefore, in the latter, the system's dynamics when it is perturbed periodically may not be approximated by 1D maps, but by two-dimensional Poincaré maps.

[26] M. Kawato and R. Suzuki, Biol. Cybern. **30**, 241 (1978); M. Kawato, J. Math. Biol. **12**, 13 (1981).

[27] K. Yoshino, T. Nomura, K. Pakdaman, and S. Sato, IEICE Technical Report No. MBE97-11, p. 75, 1997 (unpublished).